

## Article

# Comparative Analysis of Heat Transfer in a Type B LNG Tank Pre-Cooling Process Using Various Refrigerants

Qiang Sun<sup>1</sup>, Yanli Zhang<sup>1</sup>, Yan Lv<sup>1</sup>, Dongsheng Peng<sup>1</sup>, Siyu Zhang<sup>2</sup>, Zhaokuan Lu<sup>3,\*</sup> and Jun Yan<sup>2,3</sup>

<sup>1</sup> Dalian Shipbuilding Industry Co., Ltd., Dalian 116005, China; sun\_qiang@dsic-design.cn (Q.S.); dongsheng638@126.com (D.P.)

<sup>2</sup> State Key Laboratory of Structural Analysis for Industrial Equipment, School of Mechanics and Aerospace Engineering, Dalian University of Technology, Dalian 116024, China

<sup>3</sup> Ningbo Institute of Dalian University of Technology, Ningbo 315016, China

\* Correspondence: luzk\_nbi@dlut.edu.cn

**Abstract:** This study presents a comprehensive three-dimensional Computational Fluid Dynamics (CFD) analysis of the pre-cooling process of a Type B LNG tank using various refrigerants, including liquid nitrogen (LN), nitrogen gas (NG), liquefied natural gas (LNG), boil-off gas (BOG), and their combinations. The simulation model accounts for phase change (through the mixture multiphase model), convective heat transfer, and conjugate heat exchange between the fluid and the tank structure. The results indicate that liquid nitrogen is the most efficient refrigerant, achieving the highest cooling rate through both latent and sensible heat. LNG also demonstrated a relatively high cooling rate, 79% of that of liquid nitrogen. Gas-only pre-cooling schemes relying solely on sensible heat exhibited slower cooling rates, with BOG achieved 79.4% of the cooling rate of NG. Mixed refrigerants such as NG + LN and BOG + LNG can achieve comparable, while slightly slower, cooling than the pure liquid refrigerants, outperforming gas-only strategies. A further assessment of the heat transfer coefficient suggests the mixed cooling schemes have almost identical heat transfer coefficient on the inner tank surface to the liquid cooling scheme, over 5% higher than the gas refrigerants. The study also highlighted the uneven temperature distribution within the tank due to the bulkhead's blockage effect, which can induce significant thermal stress and potentially compromise structural integrity. Mixed schemes exhibit thermal gradients higher than those of gas schemes but lower than those of liquid schemes, while achieving cooling speeds comparable to liquid schemes if the inlet velocity of the refrigerants is properly configured. These findings offer valuable insights for developing safer and more efficient pre-cooling procedures for Type B LNG tanks and similar cryogenic storage tanks.

**Keywords:** LNG; IMO type B tank; cryogenic tank; pre-cooling; heat transfer; thermal stress



**Citation:** Sun, Q.; Zhang, Y.; Lv, Y.; Peng, D.; Zhang, S.; Lu, Z.; Yan, J. Comparative Analysis of Heat Transfer in a Type B LNG Tank Pre-Cooling Process Using Various Refrigerants. *Energies* **2024**, *17*, 4013. <https://doi.org/10.3390/en17164013>

Academic Editor: Fabio Polonara

Received: 5 July 2024

Revised: 28 July 2024

Accepted: 2 August 2024

Published: 13 August 2024



**Copyright:** © 2024 by the authors. Licensee MDPI, Basel, Switzerland. This article is an open access article distributed under the terms and conditions of the Creative Commons Attribution (CC BY) license (<https://creativecommons.org/licenses/by/4.0/>).

## 1. Introduction

The Type B LNG tank, classified by the International Maritime Organization, is a widely used independent tank for LNG storage and transportation. Featuring a prismatic shape and supported by a partial secondary barrier, it can be installed on various types of vessels, such as LNG carriers, floating storage and regasification units (FSRUs), and floating LNG (FLNG) platforms. The partial secondary barrier is designed to contain any potential leaks from the primary barrier, ensuring additional safety. The tank is also equipped with internal bulkheads, which help to reduce liquid sloshing, enhancing the structural integrity and stability during transport [1–3]. The Type B LNG tank offers several advantages, including high flexibility, safety, reliability, and a low cost. However, it also faces technical challenges, particularly during the pre-cooling process. Pre-cooling is a necessary step before loading LNG into cryogenic equipment, aiming to reduce the container's temperature to a level close to the LNG boiling point [4]. This practice helps prevent excessive thermal stress due to rapid temperature decreases and excessive pressure rises due to violent LNG evaporation during initial filling, which can cause safety hazards

and operational difficulties. If not properly managed, excessive stress can lead to tank wall crack [5], followed by LNG leakage, posing significant risks to both the vessel and the surrounding environment, such as explosions and pool fires [6,7]. Additionally, such hazards can endanger the safety of crew members working on board, exposing them to potential asphyxiation and frostbite [8]. Another aspect of LNG tank pre-cooling and other applications leveraging cold energy is the operation efficiency, which involves optimizing the refrigerant usage and cooling speed [9].

The pre-cooling process typically involves spraying refrigerants into the tank, such as liquid nitrogen, nitrogen gas, LNG, or boil-off gas (BOG) [10]. Unlike simple heat exchange, pre-cooling with liquid refrigerants involves complex heat and mass transfer through heat convection and phase change. Several factors affect the heat and mass transfer mechanisms during pre-cooling, including the refrigerant type, flow rate, initial temperature, and tank geometry. Most field operators manually adjust the refrigerant valve to maintain the average temperature drop, as measured by scattered thermal monitors, below 5 or 10 degrees per hour. This heuristic approach can lead to a sudden temperature drop, which creates high local temperature gradients and thermal stress. To mitigate this issue and optimize the pre-cooling process, it is essential to understand the heat transfer characteristics of various refrigerants for Type B LNG tanks.

The Type B LNG tank can be broadly categorized as a kind of cryogenic storage tank. The process of pre-cooling these cryogenic liquid storage tanks has been investigated by many researchers primarily using theoretical and numerical methods due to the difficulty of conducting cryogenic experiments. Among the models used to assess the pre-cooling process, theoretical models are the most efficient for predicting dynamic temperature and pressure variations. These models are based on the energy balance of the latent and sensible heat of the cooling medium and the heat loss by the cryogenic tank structure [11–13]. The assumption is that the temperature and pressure of the fluid in the tank and the tank structure are uniformly distributed. However, this renders the theoretical models limited, as they cannot account for local pressure and temperature gradients, which can lead to excessive stress on the tank wall. Local temperature gradients can lead to thermal stress that exceeds the yield strength of the structure, as observed in numerous cryogenic applications [14–16]. Even if the stress does not exceed yield strength, cyclic pre-cooling operations can cause thermal fatigue. Pressure caused by the evaporation of the refrigerant can also induce local stress concentration [17,18], which, while potentially lower than thermal stress, might still be significant [19]. Three-dimensional numerical modeling, specifically Computational Fluid Dynamics (CFD), allow detailed physical information such as local temperature and pressure during the pre-cooling process to be calculated, potentially offering a higher local accuracy than theoretical models due to the absence of a uniform distribution assumption.

As a result, numerical methods have become increasingly popular with advancements in computational power. Thermal stress induced by local temperature gradients has drawn the most attention in past studies. Kang et al. [20,21] assessed the cooldown characteristics and distribution of thermal stress during the filling of large-scale cryogenic tanks, finding that thermal stress on the tank wall is proportional to the cooling rate and peaks as the liquid nitrogen passes by. Lu et al. [22] conducted an LNG liquid phase pre-cooling simulation of a membrane tank and found that the temperature gradient is greatest on the innermost layer of the tank, indicating that thermal stress should be given sufficient attention to avoid tank wall damage. Chen et al. [23] performed an LNG liquid-phase pre-cooling analysis of the re-condenser in an LNG receiving station, discovering that the fatigue life of the nozzle, where thermal stress is maximum, cannot meet fatigue life requirements if the temperature drop rate exceeds 10 °C/s.

Recent years have also seen growing interest in the optimization of the pre-cooling process, with the aim of improving safety and cost efficiency. Shin et al. [24] introduced a model predictive control system that uses a reduced-order model and optimization approach to regulate temperature drop and pressure buildup during the pre-cooling of a

membrane-type LNG tank. Lim et al. [25] optimized the injection flow rate of cryogenic CO<sub>2</sub> gas used for pre-cooling CO<sub>2</sub> storage tanks on ships to minimize CO<sub>2</sub> loss. Kulitsa and Wood [26] proposed spraying LNG into the membrane LNG tank at very low rates so that the boil-off gas (BOG) generated during the pre-cooling can be utilized by the ship's engine system instead of being wasted.

However, most existing studies on the pre-cooling process of Type B LNG tanks and other cryogenic tanks have tested only one refrigerant, lacking a comprehensive comparison of the pre-cooling properties of different refrigerants. Therefore, there is a need for a systematic investigation into the pre-cooling process of the Type B LNG tank using various refrigerants, which can provide guidance for the optimal selection and design of the pre-cooling operation. In this paper, we present a CFD assessment of the pre-cooling process of Type B LNG tanks using several refrigerants: liquid nitrogen, nitrogen gas, LNG, BOG, and their combinations. The simulation model considers the effects of phase change, convective heat transfer, and conjugate heat exchange between the fluid in the tank and the tank structure. The simulation results show the temporal variation and distribution of temperature, as well as the heat transfer coefficient at the tank wall. The results illustrate how each refrigerant differs in pre-cooling properties, such as cooling efficiency and the threat to structural integrity. This paper provides guidance for selecting the optimal refrigerant and optimizing the pre-cooling operation for Type B LNG tanks and similar cryogenic storage tanks.

## 2. Model and Methodology

In this section, we describe the methodology for the CFD simulation of the Type B LNG tank pre-cooling process using four different refrigerants: liquid nitrogen, nitrogen gas, LNG, and BOG. ANSYS FLUENT 2023R1 [27] is employed to solve the physical models. We first introduce the simulation model, including the geometry, governing equations, boundary conditions, and numerical schemes. Subsequently, we validate the flow simulation model using a benchmark case to ensure accuracy and reliability of the results.

### 2.1. Model Setup

A symmetrical model of a Type B LNG tank, measuring 21 m × 28 m × 23 m and equipped with internal transverse and longitudinal bulkheads, was used for the simulation (Figure 1). The tank features a thermal insulation layer, 400 mm thick, made of expandable polystyrene (EPS) outside the inner tank layer, which is composed of 12 mm thick 9% nickel steel. Nine velocity inlets are configured at the tank top, simulating the circular droplet cloud formed by spray nozzles using 2 m diameter carved pipes, as shown in Figure 2. Additionally, a 4 m diameter pipe outlet is located at the top surface of the tank to vent the refrigerant.

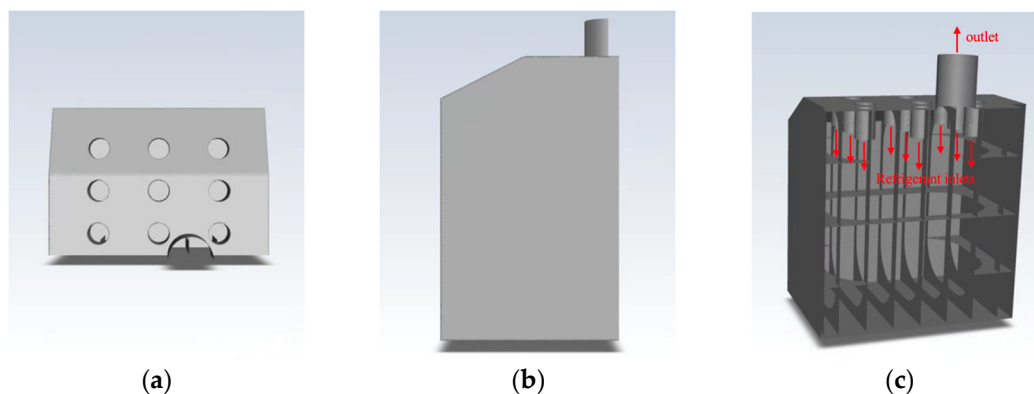


**Figure 1.** The geometry of symmetrical Type B LNG tank: (a) top view, (b) side view, and (c) isometric view.

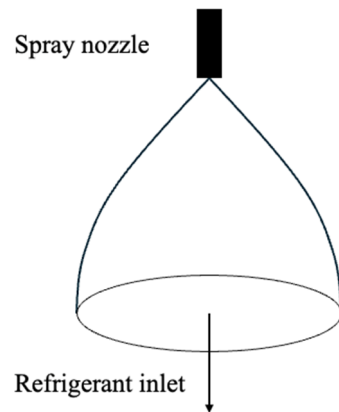


**Figure 2.** Illustration of refrigerant inlet boundary.

## 2.2. Numerical Models

For gas refrigerants (i.e., nitrogen gas and BOG), standard single-phase mass, momentum, and energy conservation equations were employed to simulate the dynamic flow and heat transfer process in the tank. On the other hand, two-phase flow caused by the rapid evaporation of the liquid refrigerants (i.e., liquid nitrogen and LNG) was simulated using a combination of the mixture model and the standard k-epsilon model with enhanced wall functions. The reason for employing the mixture model is that the liquid refrigerant injected into the tank by spray nozzles is typically in the form of fine droplets, which are small enough to follow the motion of the bulk flow. The gas and liquid phases are assumed to interact strongly, with little relative velocity (neglected in the current investigation). Therefore, the mixture model simplifies the analysis by solving a single momentum equation for the combined phases, rather than solving separate momentum equations for each phase, greatly improving the computational efficiency. This type of model is also referred to as a homogeneous Eulerian model and is frequently used for spray and leakage two-phase flow simulation (e.g., [28–30]),

$$\frac{\partial}{\partial t}(\rho_m) + \nabla \cdot (\rho_m \vec{v}_m) = 0 \quad (1)$$

in which  $\vec{v}_m$  is the mass-averaged velocity and  $\rho_m$  is the mixture density:

$$\vec{v}_m = \frac{\sum_{i=1}^n \alpha_i \rho_i \vec{v}_i}{\rho_m} \quad (2)$$

$$\rho_m = \sum_{i=1}^n \alpha_i \rho_i \quad (3)$$

where  $\alpha_i$  is the volume fraction of phase  $i$ . In this work, we set the liquid to be the primary phase ( $l$ ) and vapor to be the secondary phase ( $v$ ). The continuity equation for the secondary phase can be expressed as:

$$\frac{\partial}{\partial t}(\alpha_v \rho_v) + \nabla \cdot (\alpha_v \rho_v \vec{v}_m) = \sum_{q=1}^n (\dot{m}_{lv} - \dot{m}_{vl}) \quad (4)$$

where  $\dot{m}_{lv}$  is the rate of mass transfer from primary to secondary phase, and  $\dot{m}_{vl}$  is the rate of mass transfer from secondary to primary phase (expression to be defined in Equation (9)).

The momentum equation of the mixture can be written as:

$$\frac{\partial}{\partial t}(\rho_m \vec{v}_m) + \nabla \cdot (\rho_m \vec{v}_m \vec{v}_m) = -\nabla \left( P + \frac{2}{3} \rho_m k \right) + \nabla \cdot \left[ (\mu_m + \mu_T) \left( \nabla \vec{v}_m + \nabla \vec{v}_m^T \right) \right] + \rho_m \vec{g} \quad (5)$$

where  $P$  is the fluid pressure and  $\mu_m$  is the viscosity of the mixture:

$$\mu_m = \sum_{i=1}^n \alpha_i \mu_i \quad (6)$$

$k$  is the turbulence kinetic energy, and  $\mu_T$  is the eddy viscosity, both created by the Boussinesq approximation to capture the effect of turbulence fluctuation.  $\mu_T$  is calculated by  $k$  and its dissipation rate  $\epsilon$  in the  $k - \epsilon$  formulation as:

$$\mu_t = \rho C_\mu \frac{k^2}{\epsilon} \quad (7)$$

where  $C_\mu$  is a constant coefficient. Two additional transport equations of  $k$  and  $\epsilon$  have to be employed to close the fluid governing equation and are omitted for brevity.

The mixture energy conservation equation is used to model the heat transfer process during the liquid pre-cooling:

$$\frac{\partial}{\partial t} \sum_i \alpha_i \rho_i E_i + \nabla \cdot \sum_i \left( \alpha_i \vec{v}_i (\rho_i E_i + P) \right) = \nabla \cdot \left( k_{eff} \nabla T + \vec{\tau}_{eff} \cdot \vec{v}_m \right) + S_h \quad (8)$$

where the left-hand side represents the collective energy transfer due to convective transfer of each phase  $i$ ; the first and second term on the right-hand side are the energy transfer caused by thermal conduction and viscous dissipation; the last term  $S_h$  is the volumetric heat source by the evaporation of the liquid refrigerant, which can be expressed by  $S_h = \dot{m}_{lv} L_v$ , where  $L_v$  is the latent heat of the liquid refrigerant; and  $\dot{m}_{lv}$  is the rate of mass transfer from liquid phase (primary) to vapor phase (secondary), estimated using the Lee model:

$$\begin{aligned} \dot{m}_{lv} &= coeff * \alpha_l \rho_l \frac{T_l - T_{sat}}{T_{sat}}, \text{ if } T_l > T_{sat} \\ \dot{m}_{vl} &= coeff * \alpha_v \rho_v \frac{T_{sat} - T_v}{T_{sat}}, \text{ if } T_l < T_{sat} \end{aligned} \quad (9)$$

where  $coeff$  is an empirical coefficient, set to 0.1 based on comparable published studies [22,31];  $T_l$  and  $T_{sat}$  are the phase temperature and saturation temperature of the liquid refrigerants. A user-defined function (UDF) was used to dynamically calculate  $T_{sat}$  under varying pressure  $P$  in each step by the Antoine equation (Equation (10)). The coefficients A, B, and C were obtained from National Institute of Standards and Technology (NIST) for nitrogen [32] and BOG (assumed to be pure methane) [33], as shown in Table 1. The physical properties of methane and nitrogen used in this investigation can be found in Appendix A. The tank was assumed to be initially filled by gas of the same chemical component as the refrigerant, with a temperature of 25 °C.

$$T_{sat} = \frac{B}{A - \log_{10} P} - C \quad (10)$$

**Table 1.** Coefficients of Antoine equation.

	A	B	C
Nitrogen	3.7362	264.651	−6.788
BOG	3.9895	443.028	−0.49

A normal flow velocity and zero-gauge pressure boundary conditions were prescribed to the aforementioned tank inlets and outlet, respectively.

The energy conservation equation for a solid was employed to calculate the temperature variation in tank structure. The conjugate heat transfer boundary condition was applied to the inner surface of the 9% nickel steel layer (inner tank layer). Given the large dimensional difference between the thickness and the surface of the inner tank layer, the shell conduction model was used for the inner layer, while the outer layer (EPS layer)

was explicitly modeled for heat conduction. A heat transfer coefficient of  $5 \text{ W/m}^2 \cdot ^\circ\text{C}$  and an environment temperature of  $25 \text{ }^\circ\text{C}$  were prescribed to the outer surface of the tank to consider the natural heat convection of the external fluid.

For temporal and spatial discretization, a constant time step size of 10 s was used, with the Pressure-Implicit with Splitting of Operators (PISO) algorithm to implicitly advance the simulation over time by a convergence criterion of  $1 \times 10^{-4}$ . A mesh composed of polyhedral elements generated by FLUENT was used for spatial discretization. The mesh independence criterion was based on the convergence of the average temperature of the inner tank layer. More details on the mesh setup and mesh independence study can be found in Appendix B.

### 2.3. Model Validation

A BOG dispersion simulation replicating the experimental results of the Burro series test by the National Renewable Energy Laboratory (NREL) [34] was performed to verify the reliability of using the standard k-epsilon turbulence model with enhanced wall function for large-scale non-isothermal gas dispersion analysis, which is crucial for the LNG tank pre-cooling process. The Burro series test, conducted in 1980, studied the dispersion and flammability of BOG released from LNG spills on a lake. The test involved a series of experiments with different spill sizes, release rates, and wind speeds, providing valuable data for validating numerical models of BOG dispersion behavior.

In this section, we describe a case following the setup by Bellegoni et al. [35], who proposed using BOG inlet conditions to represent LNG spillage on a lake surface. The simulation domain had dimensions of  $500 \text{ m} \times 200 \text{ m} \times 35 \text{ m}$ , with an inlet pool diameter of 13.6 m and a BOG mass flow rate of  $113 \text{ kg/s}$  at  $-162 \text{ }^\circ\text{C}$ . The air inlet boundary condition was set with a wind speed of  $1.8 \text{ m/s}$ , and a zero-gauge pressure outlet boundary condition was applied (see Figure 3). The ground was set as a non-slip boundary condition, while the rest of the boundaries were set to be symmetrical.

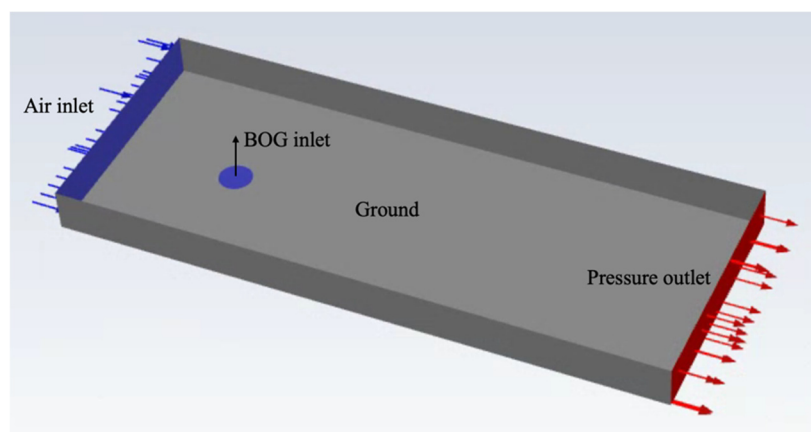


**Figure 3.** Gas dispersion model setup.

The volume concentration of BOG (i.e., methane) at a 1 m height is shown in Figure 4 and a comparison of the spatial location with 5% and 10% BOG concentrations with the experimental results is shown in Figure 5. The comparison suggests that the model used in this work can adequately capture the dispersion behavior of low-temperature gas in environment with ambient temperature, although the accuracy may decline as the gas concentration decreases.

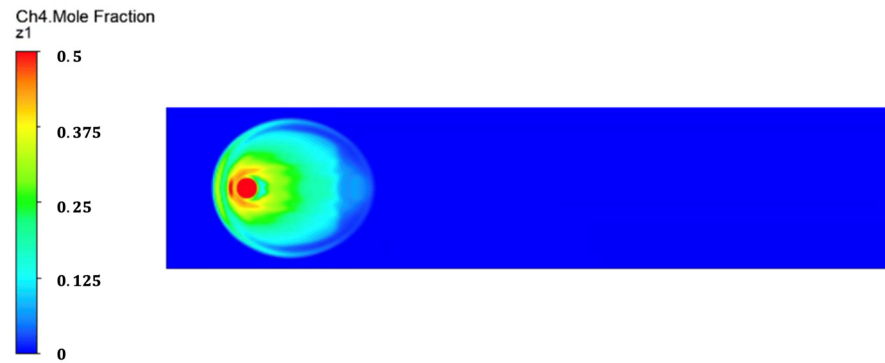


Figure 4. Contour plot of BOG concentration at 1 m height.

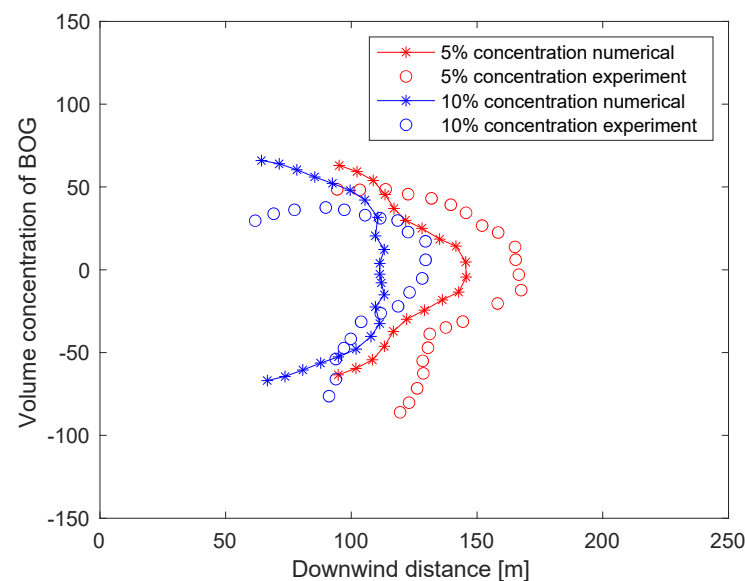


Figure 5. Comparison between numerical and experimental results.

### 3. Results and Discussion

In this section, the results of the transient LNG B-type tank pre-cooling simulations performed using the numerical model described in Section 2 are outlined. Six pre-cooling schemes using liquid nitrogen (LN), nitrogen gas (NG), NG + LN, LNG, BOG, and BOG + LNG are assessed. The mixed pre-cooling schemes (Case 3 and Case 6) cool the tank first with cryogenic gas before injecting the liquid refrigerant to continue the pre-cooling, a practice frequently used in LNG receiving stations. In the current simulation, the solutions in Case 2 (NG) and Case 5 (BOG) at 5.8 h were used as the initial conditions for Case 3 and Case 6, respectively, while the inlet liquid refrigerant flow velocity was kept the same as in Case 1 (LN) and Case 4 (LNG).

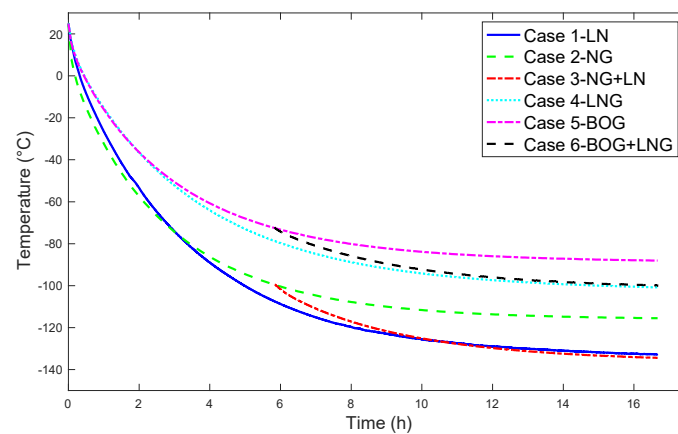
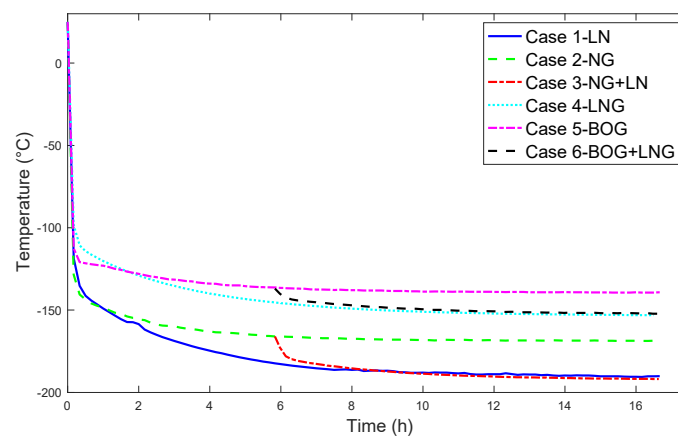
The flow rate and temperature of the refrigerants are listed in Table 2. The flow rates were selected to allow the pre-cooling of all schemes to complete within roughly the same duration (when the temperature stops varying significantly), with the gas refrigerants and liquid refrigerants each maintaining consistent flow rates. In the following subsections, temperature variation, temperature distribution, and temperature gradient are compared to evaluate the different cooling schemes.

**Table 2.** Flow rate and temperature of refrigerants in different cases.

Case	Flow Rate [m/s]	Refrigerant Temperature [°C]
1 (LN)	$2.45 \times 10^{-4}$	−195
2 (NG)	$7.72 \times 10^{-4}$	−180
3 (NG + LN)	$2.45 \times 10^{-4}$	−195
4 (LNG)	$2.45 \times 10^{-4}$	−162
5 (BOG)	$7.72 \times 10^{-4}$	−150
6 (BOG + LNG)	$2.45 \times 10^{-4}$	−162

### 3.1. Temperature Variation

The variation in the average temperature of the inner tank layer and the bulkhead is shown in Figures 6 and 7, respectively. The trend suggests that the cooldown rate of the tank structure gradually decreases as pre-cooling proceeds, with the bulkhead cooling more quickly than the inner layer. This can be attributed to the decreased heat flux resulting from the reduced temperature difference between the tank structure and the refrigerant as the pre-cooling progresses. Meanwhile, the variation in the average temperature of the fluid inside the tank, shown in Figure 8, decreases at a much faster rate, reaching a steady state more quickly. This rapid fluid cooling contributes to the faster cooling rate of the bulkhead, which is immersed in the refrigerant, unlike the inner tank layer.

**Figure 6.** Comparison of inner tank layer temperature variation under different pre-cooling schemes.**Figure 7.** Comparison of bulkhead temperature variation under different pre-cooling schemes.



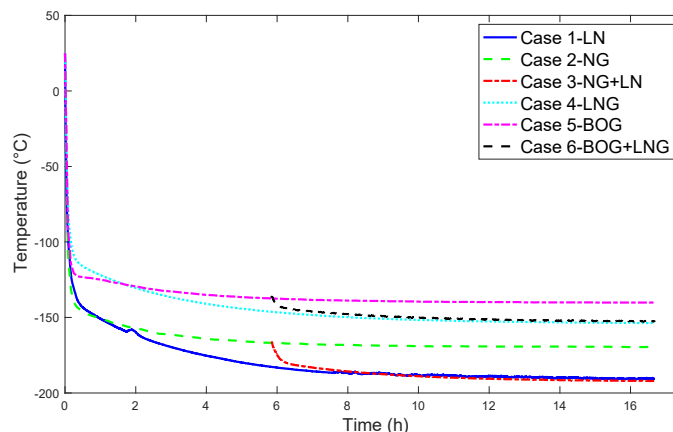


**Figure 8.** Comparison of fluid temperature variation under different pre-cooling schemes.

Liquid refrigerants, specifically liquid nitrogen (LN) in Case 1 and liquefied natural gas (LNG) in Case 4, demonstrate a superior cooling performance compared to gas refrigerants with the same chemical component. Case 1 (LN) achieves the fastest initial temperature drop of the inner tank layer, reaching below  $-100\text{ }^{\circ}\text{C}$  within 8 h and stabilizing around  $-140\text{ }^{\circ}\text{C}$  by 16 h. In comparison, Case 4 (LNG) shows a rapid initial cooldown similar to Case 1 but levels off at  $-120\text{ }^{\circ}\text{C}$  after 10 h. The normalized mean temperature drop rate at each sampled time (calculated by trapezoidal rule) until 8 h is listed in Table 3, which suggests that the cooling rate of LNG is only 79% of that of LN. The difference in performance between LN and LNG can be attributed to their distinct thermophysical properties. Liquid nitrogen, with its extremely low boiling point of  $-195\text{ }^{\circ}\text{C}$ , provides a very high temperature difference between the refrigerant and the tank, driving faster and more substantial heat transfer. This results in a more rapid initial cooldown and a lower final temperature. In contrast, LNG, with a boiling point of around  $-162\text{ }^{\circ}\text{C}$ , has a higher initial temperature compared to LN. While still effective, the smaller temperature difference between LNG and the tank results in a slower heat transfer rate, leading to a higher final temperature compared to LN.

**Table 3.** Normalized temperature drop rate of inner tank layer until 8 h (normalized using the result for Case 1).

Case	Normalized Temperature Drop Rate
1 (LN)	1
2 (NG)	0.92
3 (NG + LN)	0.98
4 (LNG)	0.79
5 (BOG)	0.73
6 (BOG + LNG)	0.77

For gas refrigerants, Case 2 (NG) exhibits a slower cooldown rate compared to liquid nitrogen, reaching only about  $-115\text{ }^{\circ}\text{C}$  after 16 h. This slower cooling rate can be attributed to the higher initial temperature and absence of latent heat, which has a significant contribution to liquid pre-cooling process. Case 5 (BOG) shows a similar cooling pattern to NG but with 79.4% of its cooling rate (as calculated from results in Table 3). The performance difference between NG and BOG can also be explained by the lower initial temperature of BOG, which leads to a smaller heat transfer rate on the tank surface.

The gas–liquid mixed cooling schemes, Case 3 (NG + LN) and Case 6 (BOG + LNG) reach steady state at approximately the same time as the pure liquid pre-cooling, despite the difference in temperature as the liquid phase cooling starts. Overall, liquid nitrogen and LNG facilitated the most rapid cooldown. The mixed schemes, while slightly slower,

achieved comparable cooling rates. The gas-only refrigerants exhibited the slowest cooling rates and the highest steady-state temperatures among the cases investigated.

To further compare the efficiency of different pre-cooling schemes, the average heat transfer coefficients (HTC) on the inner tank surface were obtained and are shown in Figure 9, and their mean values over the simulation period are listed in Table 4. HTC is an important indicator of the effectiveness of heat transfer between the refrigerant and the tank surface. The liquid refrigerants (Case 1 and Case 4) exhibited higher HTCs than their pure gas counterparts (Case 2 and Case 5). The HTCs continued to increase, albeit at a slower rate, as cooling progressed. In contrast, the gas refrigerants (Case 2 and Case 5) reached a plateau before decreasing, showing 8% and 7% lower mean HTCs (calculated from Table 4). This difference arises from the distinct cooling mechanisms of the two types of refrigerants. Cryogenic liquids benefit from latent heat during evaporation and both forced and natural convection of the evaporated gas and liquid. As evaporation diminishes due to lower tank temperatures, the remaining liquid still significantly contributes to heat transfer. Gas refrigerants, on the other hand, rely solely on sensible heat through forced and natural convection. Liquids achieve much larger heat transfer coefficients than gasses due to their higher thermal conductivity, leading to the continuous rise in the heat transfer coefficient for liquid refrigerants. Despite having greater thermal conductivity, LNG shows a 16% lower heat transfer coefficient than liquid nitrogen at the same inlet velocity (calculated from Table 4). This is due to the lower temperature of its evaporated gas (i.e., BOG), which leads to weaker natural heat convection, primarily driven by the temperature gradient at the tank wall. The same rationale can account for the relative difference between the two gas refrigerants (Case 2 (NG) and Case 5 (BOG)). For the mixed strategies (Case 3 and Case 6), the heat transfer coefficient quickly matches the level of pure liquid refrigerants, aligning with the temperature variation trends shown in Figure 6. As indicated in Table 4, the mean heat transfer coefficient is also approximately the same as that of pure liquid refrigerants.

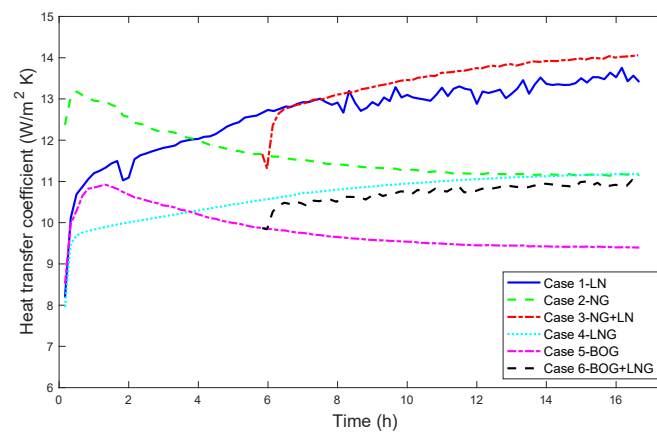


**Figure 9.** Comparison of the heat transfer coefficient variation on the inner tank surface under different pre-cooling schemes.

**Table 4.** Normalized mean HTC on the inner tank surface over the simulation period (normalized by result of Case 1).

Case	Normalized HTC
1 (LN)	1
2 (NG)	0.92
3 (NG + LN)	1.04
4 (LNG)	0.84
5 (BOG)	0.78
6 (BOG + LNG)	0.84

### 3.2. Temperature Distribution

To examine the temperature distribution within the tank during the pre-cooling process, temperature contour plots of the inner tank surface and bulkhead for different cooling schemes at 1 h into the pre-cooling process were extracted and are shown in Figure 10. For all the cases assessed, the temperature distribution of the bulkhead is more uniform than that of the inner tank surface, which exhibits lower surface temperatures above the center transverse bulkhead than below it, creating a vertical temperature gradient on the side surface. The temperature of the tank's bottom surface drops faster than that of the side surfaces, with the top surface temperature remaining the highest.

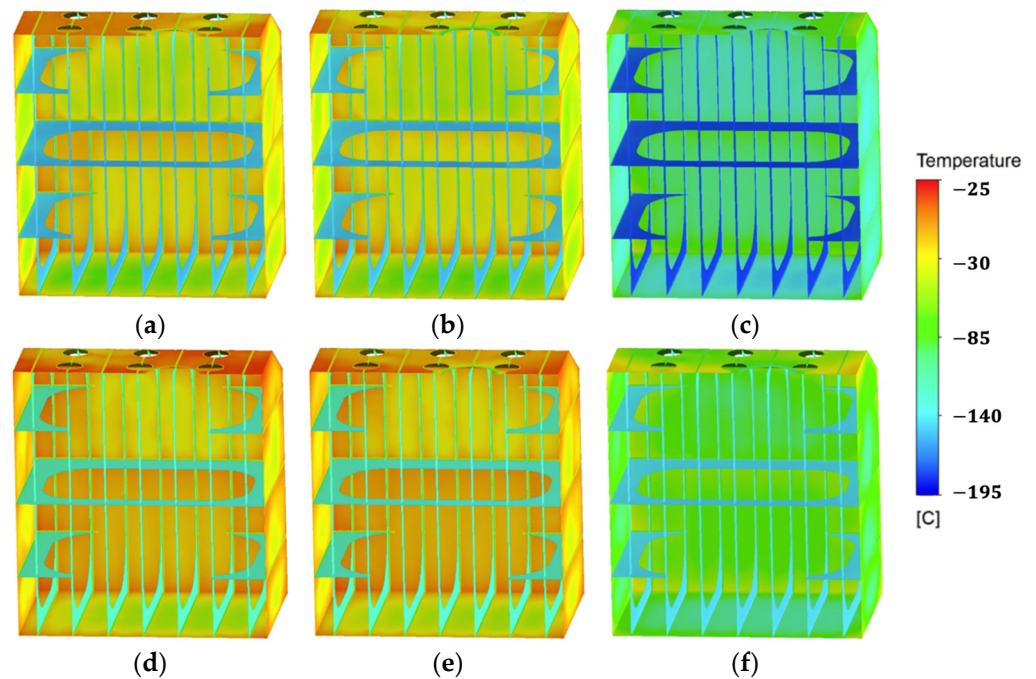


**Figure 10.** Temperature distribution of the tank structure under different pre-cooling schemes after an hour into the pre-precooling process. (a) Case 1 (LN), (b) Case 2 (NG), (c) Case 3 (NG + LN), (d) Case 4 (LNG), (e) Case 5 (BOG), (f) Case 6 (BOG + LNG).

The pattern of a non-uniform temperature distribution on the inner tank surface can be explained by the velocity magnitude contour and streamline plot sampled at a YZ plane (shown in Figure 11). The streamlines in Figure 12 suggest that the refrigerants injected into the tank reach the bottom first, forming two nearly symmetric vortices that circulate the flow upwards along the side surfaces. As a result, the refrigerant stream arriving at the side surfaces has already lost some of its cold energy, causing slower cooling. Additionally, the center transverse bulkhead exerts a blocking effect on the inlet refrigerant flow, effectively dividing the tank into two flow regions, upper and lower. This observation helps to explain the uneven vertical temperature distribution on the inner tank surface. It is worth noting that the bulkhead, used to prevent liquid sloshing, is a key feature distinguishing the Type B LNG tank from other LNG tanks [36,37]. As a result, the Type B LNG tanks may be more prone to an uneven temperature distribution (and therefore thermal stress problems) compared to the other types of LNG tanks.

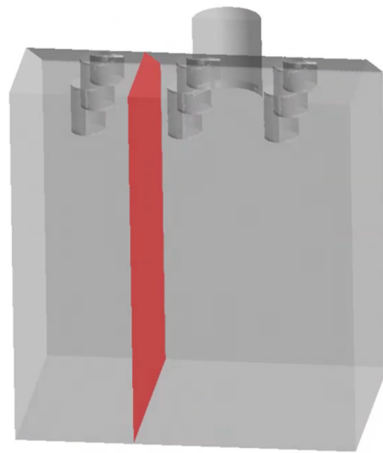


**Figure 11.** Flow velocity sampling plane.

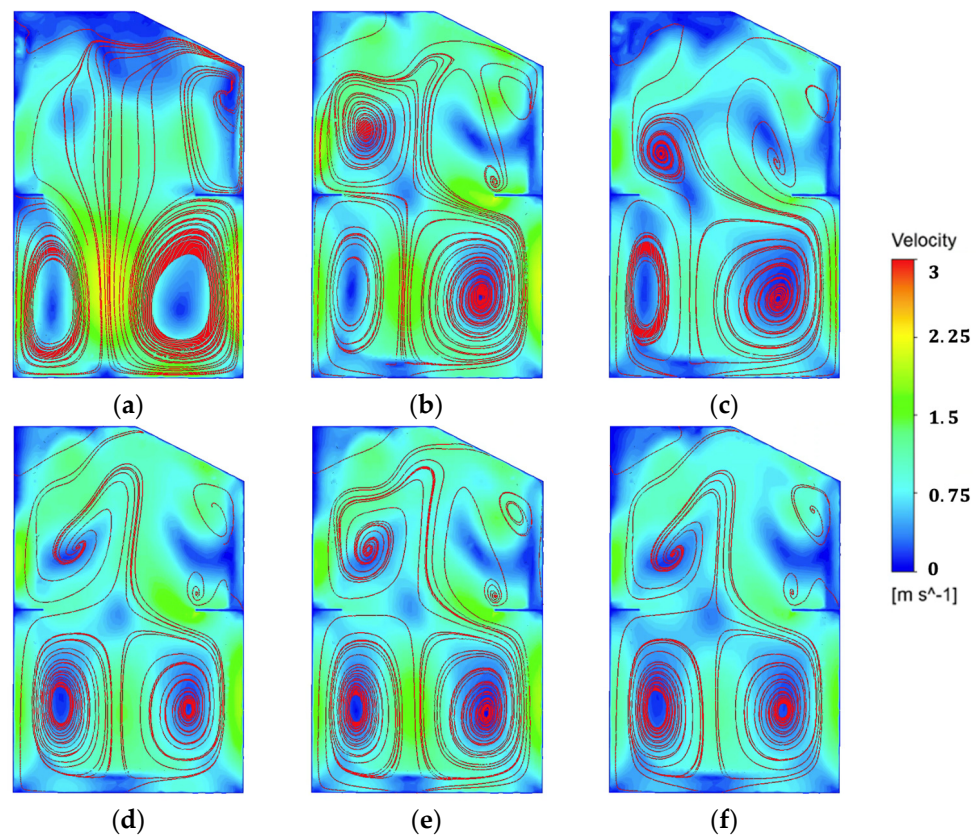


**Figure 12.** Flow velocity and streamline visualization at the sampled plane under different pre-cooling schemes after an hour into the pre-cooling process. (a) Case 1 (LN), (b) Case 2 (NG), (c) Case 3 (NG + LN), (d) Case 4 (LNG), (e) Case 5 (BOG), (f) Case 6 (BOG + LNG).

### 3.3. Temperature Gradient

In light of the uneven temperature distribution within the tank structure, we have extracted the transient variation of the average temperature gradient magnitude of the inner tank layer and bulkhead, which is an important indicator of the level of thermal stress during the pre-cooling process. Figures 13 and 14 show a comparison of the temperature gradients for the different pre-cooling schemes. It is evident that the temperature gradient of the bulkhead is significantly smaller than that of the inner tank layer, which can be attributed to the more uniform cooling observed in Figure 10.

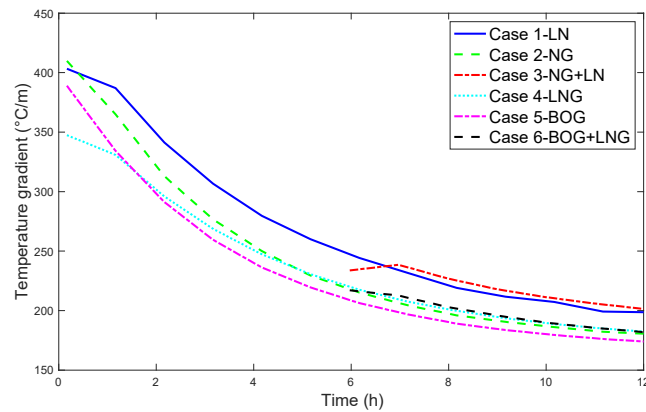


**Figure 13.** Comparison of transient temperature gradient of inner tank surface under different pre-cooling schemes.

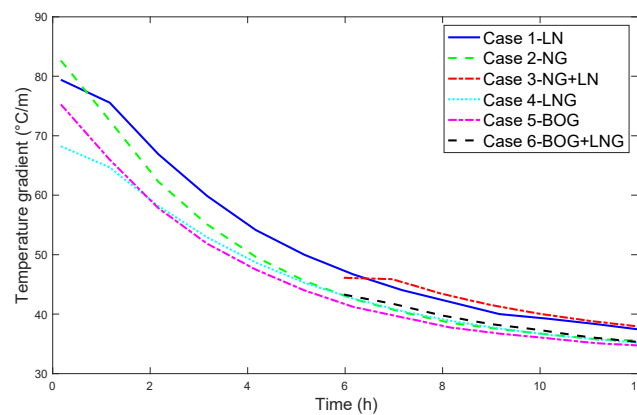


**Figure 14.** Comparison of transient temperature gradient of bulkhead under different pre-cooling schemes.

For different pre-cooling schemes, the relative magnitudes of the temperature gradient are consistent between the inner tank layer and bulkhead (see Tables 5 and 6) and aligned with the structure cooling rate presented in Section 3.1. Among all the schemes, Case 5 (BOG) exhibits the lowest overall temperature gradient, followed by Case 4 (LNG) and Case 6 (BOG + LNG). The schemes using liquid nitrogen and nitrogen gas result in larger temperature gradients, with Case 1 (LN) and Case 3 (NG + LN) showing higher gradients than Case 2 (NG). It is noteworthy that the mixed cooling scheme can achieve a comparable cooling rate (as illustrated in Section 3.1) while maintaining a smaller, if not similar, temperature gradient compared to the pure liquid cooling scheme, provided the inlet velocity of the refrigerants is properly controlled, as demonstrated in this study.

**Table 5.** Normalized mean temperature gradient of the inner tank layer over the simulation period (normalized by result of Case 1).

Case	Normalized Mean Temperature Gradient
1 (LN)	1
2 (NG)	0.917
3 (NG + LN)	0.944
4 (LNG)	0.887
5 (BOG)	0.870
6 (BOG + LNG)	0.888

**Table 6.** Normalized mean temperature gradient of the bulkhead over the simulation period (normalized by result of Case 1).

Case	Normalized Mean Temperature Gradient
1 (LN)	1
2 (NG)	0.942
3 (NG + LN)	0.957
4 (LNG)	0.898
5 (BOG)	0.896
6 (BOG + LNG)	0.908

#### 4. Conclusions

CFD simulations of the Type B LNG tank pre-cooling process using different refrigerants provide valuable insights into the thermodynamic characteristics of each cooling strategy. During the pre-cooling process, the temperature of the tank rapidly decreases before leveling off. The fluid inside the tank exhibits the fastest temperature drop, followed by the bulkheads immersed in it, while the tank hull structure shows the slowest temperature drop. Liquid nitrogen (LN) was found to be the most efficient refrigerant, achieving the highest cooling rate through both latent and sensible heat. LNG also demonstrated a relatively high cooling rate, 79% of that of the liquid nitrogen due to its higher boiling point. In contrast, gas-only pre-cooling schemes relying solely on sensible heat are less efficient, among which the cooling rate of the boil-off gas (BOG) was 79.4% of that of nitrogen gas (NG). Mixed refrigerants such as NG + LN and BOG + LNG can achieve comparable, while slightly slower, cooling rates than the pure liquid refrigerants, outperforming gas-only strategies. A further assessment of heat transfer coefficient suggests the mixed cooling schemes have almost identical heat transfer coefficient on the inner tank surface to the liquid cooling scheme, over 5% higher than the gas refrigerants.

The study also highlighted the uneven temperature distribution within the tank, particularly in the inner tank layer, due to the bulkhead's blockage effect on refrigerant flow. This uneven distribution, characterized by high local temperature gradients, can induce significant thermal stress, potentially compromising the structural integrity of the tank. Given that the bulkhead is a key feature distinguishing the LNG B-type tank from other LNG tanks, this type of tank may be more prone to excessive thermal stress. Among the cooling schemes assessed in this study, mixed schemes exhibit higher thermal gradient than the gas schemes but lower thermal gradient than the liquid schemes while achieving the same level of high cooling efficiency if the inlet velocities of gas and liquid refrigerants are configured properly.

In summary, the selection of refrigerants for the pre-cooling process of Type B LNG tanks should consider both cooling efficiency and the potential for thermal stress. The findings in this work can hopefully provide a basis for developing more effective and safer pre-cooling procedures for Type B LNG tanks and similar cryogenic tanks. Future research could focus on evaluating additional refrigerants, quantifying the magnitude of thermal stress under different refrigerants, and validating the results through full-scale experiments.

**Author Contributions:** Conceptualization, Z.L.; Investigation, Q.S., Z.L. and Y.L.; Data curation, Y.Z.; Software, Q.S.; Validation, Y.Z.; Methodology, Q.S.; Visualization, S.Z.; Writing—original draft, Q.S., Y.Z., Y.L., Z.L.; Writing—review and editing, S.Z.; Resources, D.P., Y.L.; Supervision, J.Y.; Funding acquisition, J.Y.; Project administration, D.P. All authors have read and agreed to the published version of the manuscript.

**Funding:** This research was funded by the Key Research and Development Program of Dalian: 2022JB11SN008.

**Data Availability Statement:** The data presented in this study are available upon request from the corresponding author. The data are not publicly available due to privacy.

**Conflicts of Interest:** Authors Qiang Sun, Yanli Zhang, Yan Lv, and Dongsheng Peng were employed by the company Dalian Shipbuilding Industry Co., Ltd. The remaining authors declare that the research was conducted in the absence of any commercial or financial relationships that could be construed as a potential conflict of interest.

## Nomenclature

$E_i$	energy of phase $i$ (J)
$\vec{g}$	gravitational acceleration ( $\text{m}^2/\text{s}$ )
$k$	turbulence kinetic energy (J/kg)
$L_v$	latent heat of the liquid refrigerant (J/kg)
$k_{eff}$	effective thermal conductivity ( $\text{W}/\text{m}\cdot^\circ\text{C}$ )
$\dot{m}_{lv}$	mass transfer rate from liquid to vapor phase (kg/s)
$\dot{m}_{vl}$	mass transfer rate from vapor to liquid phase (kg/s)
$P$	fluid pressure (Pa)
$t$	Time (s)
$T_l$	temperature of liquid ( $^\circ\text{C}$ )
$T_{sat}$	saturation temperature of liquid ( $^\circ\text{C}$ )
$S_h$	volumetric heat source by evaporation ( $\text{W}/\text{m}^3$ )
$\vec{v}_m$	mass-averaged velocity (m/s)
Greek letters	
$\alpha_i$	volume fraction of phase $i$
$\alpha_l$	volume fraction of liquid phase
$\alpha_g$	volume fraction of vapor phase
$\rho_m$	mass-averaged density ( $\text{kg}/\text{m}^3$ )
$\rho_i$	density of phase $i$ ( $\text{kg}/\text{m}^3$ )
$\mu_m$	mixture viscosity ( $\text{Pa}\cdot\text{s}$ )
$\mu_T$	turbulence viscosity ( $\text{Pa}\cdot\text{s}$ )
$\epsilon$	turbulence dissipation rate ( $\text{m}^2/\text{s}^3$ )
$\overline{\tau}_{eff}$	effective viscous dissipation coefficient

## Appendix A

**Table A1.** Refrigerant properties.

	Nitrogen	Liquid Nitrogen	BOG	LNG
Density [ $\text{kg}/\text{m}^3$ ]	Idea gas law	804	Idea gas law	414
Molar weight [ $\text{kg}/\text{kmol}$ ]	28.014	28.014	16.04	16.04
Specific heat [ $\text{J}/\text{kg}\cdot\text{k}$ ]	1040	1040	2087	2087
Thermal conductivity [ $\text{w}/\text{m}\cdot\text{k}$ ]	see Table A2	$145 \times 10^{-3}$	see Table A4	$184.1 \times 10^{-3}$
Dynamic viscosity [ $\text{kg}/\text{m}\cdot\text{s}$ ]	see Table A3	$161.4 \times 10^{-6}$	see Table A5	$117.2 \times 10^{-6}$
Standard state enthalpy [ $\text{J}/\text{kgmol}$ ]	6,100,000	0	8,180,400	0
Critical temperature [ $^\circ\text{C}$ ]	/	−147	/	−82.1
Surface tension coefficient [ $\text{N}/\text{m}$ ]	/	0.00885	/	0.014
Reference temperature [ $^\circ\text{C}$ ]	−195	−195	−162	−162

**Table A2.** Thermal conductivity of nitrogen at different temperatures.

Temperature [ $^\circ\text{C}$ ]	Thermal Conductivity [ $\text{w}/\text{m}\cdot\text{k}$ ]
−193.2	$7.443 \times 10^{-3}$
−173.2	$9.381 \times 10^{-3}$
−153.2	$11.27 \times 10^{-3}$
−133.2	$13.11 \times 10^{-3}$
−113.2	$14.89 \times 10^{-3}$
−93.2	$16.61 \times 10^{-3}$

**Table A2.** *Cont.*

Temperature [°C]	Thermal Conductivity [w/m·k]
−73.2	$18.28 \times 10^{-3}$
−53.2	$19.90 \times 10^{-3}$
−33.2	$21.48 \times 10^{-3}$
−13.2	$23.01 \times 10^{-3}$
6.9	$24.51 \times 10^{-3}$

**Table A3.** Dynamic viscosity of nitrogen at different temperatures.

Temperature [°C]	Dynamic Viscosity [kg/m·s]
−193.2	$5.623 \times 10^{-6}$
−173.2	$6.958 \times 10^{-6}$
−153.2	$8.224 \times 10^{-6}$
−133.2	$9.480 \times 10^{-6}$
−113.2	$10.67 \times 10^{-6}$
−93.2	$11.81 \times 10^{-6}$
−73.2	$12.91 \times 10^{-6}$
−53.2	$13.97 \times 10^{-6}$
−33.2	$15 \times 10^{-6}$
−13.2	$15.99 \times 10^{-6}$
6.9	$16.96 \times 10^{-6}$

**Table A4.** Thermal conductivity of BOG (i.e., methane) at different temperatures.

Temperature [°C]	Thermal Conductivity [w/m·k]
−161.6	$11.43 \times 10^{-3}$
−133	$14.65 \times 10^{-3}$
−93.2	$19.32 \times 10^{-3}$
−73.2	$21.94 \times 10^{-3}$
−53.2	$23.99 \times 10^{-3}$
−33.2	$26.39 \times 10^{-3}$
−13.2	$28.88 \times 10^{-3}$
6.9	$31.47 \times 10^{-3}$

**Table A5.** Dynamic viscosity of BOG (i.e., methane) at different temperatures.

Temperature [°C]	Dynamic Viscosity [kg/m·s]
−161.6	$4.327 \times 10^{-6}$
−133	$5.449 \times 10^{-6}$
−93.2	$6.963 \times 10^{-6}$
−73.2	$7.697 \times 10^{-6}$
−53.2	$8.416 \times 10^{-6}$
−33.2	$9.117 \times 10^{-6}$
−13.2	$9.803 \times 10^{-6}$
6.9	$10.47 \times 10^{-6}$

## Appendix B

In this section, the independence of the polyhedral mesh used in the type B tank pre-cooling analysis is demonstrated through the variation in the average inner layer temperature. The polyhedral mesh is generated based on a uniformly spaced tetrahedral background mesh in Fluent (using the FLUENT meshing module) in Ansys Workbench, as shown in Figure A1. To determine the appropriate mesh density, three meshes with degrees of freedom (DOF) of  $4.93 \times 10^5$  (Mesh 1),  $9.85 \times 10^5$  (Mesh 2), and  $1.96 \times 10^6$



(Mesh 3) (each refinement doubling the DOF) are generated. The variation in the average temperature of the inner tank layer during pre-cooling Case 1 (the case with the most rapid temperature variation) is calculated and presented in Figure A2. As shown, the difference between Mesh 2 and Mesh 3 is smaller than that between Mesh 1 and Mesh 2, indicating convergence. This is further supported by the average absolute difference at each sampled time, which drops from 3.43 to 1.32 as the mesh is refined. Given the converging results and the minimal difference between Mesh 2 and Mesh 3, the simulations performed in Section 3 are based on Mesh 2 to save computational effort.

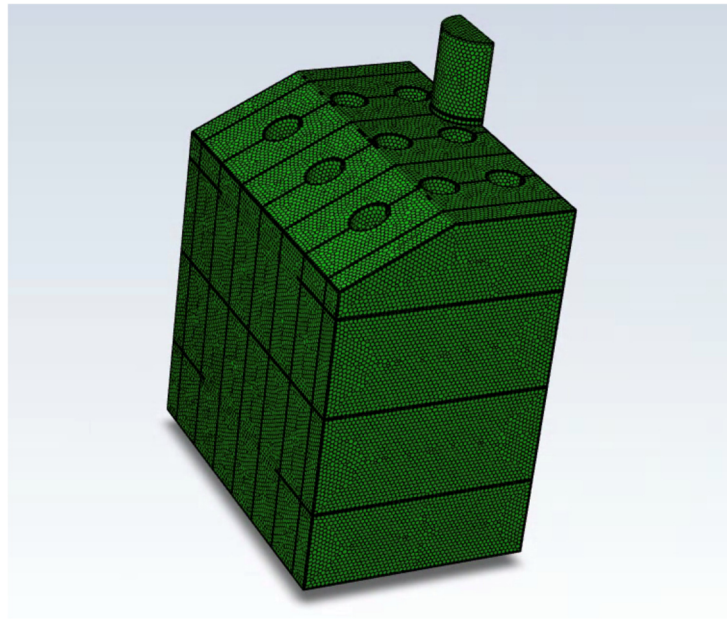


Figure A1. Polyhedral meshing of the type B LNG tank.

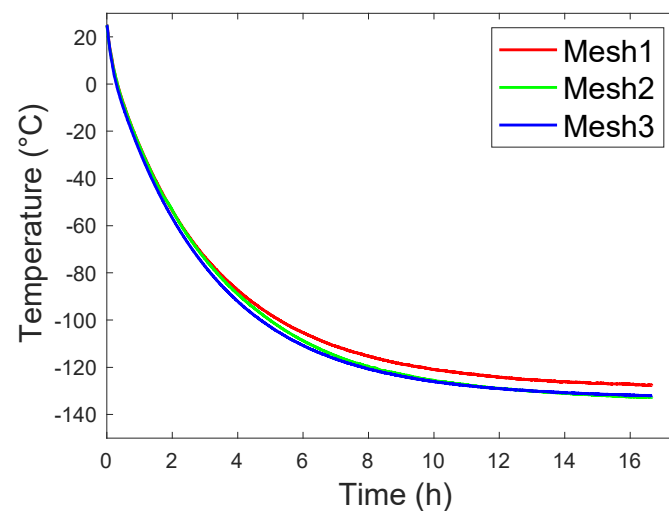


Figure A2. Comparison of inner tank layer temperature variation using meshes with different densities.

## References

1. Kim, T.W.; Kim, S.K.; Park, S.B.; Lee, J.M. Design of Independent Type-B LNG Fuel Tank: Comparative Study between Finite Element Analysis and International Guidance. *Adv. Mater. Sci. Eng.* **2018**, *2018*, 5734172. [[CrossRef](#)]
2. Kim, B.I.; Islam, S. Development of Design Procedure for LNG Carriers with IMO Type-B Independent Tank. In Proceedings of the International Conference on Offshore Mechanics and Arctic Engineering—OMAE, Hamburg, Germany, 5–11 June 2022; Volume 1.

3. Seo, J.H.; Park, K.-S.; Cha, I.; Choung, J. Engineering Critical Assessment for an Independent Type-B LNG Cargo Tank. *J. Soc. Nav. Archit. Korea* **2023**, *60*, 213–221. [[CrossRef](#)]
4. Zhu, J.; Zheng, B.; Wang, S.; Li, Q.; Wang, H. Boil-off Gas Precooling Process for Subsea Low Temperature LNG Pipelines. *Sustain. Horiz.* **2023**, *8*, 100070. [[CrossRef](#)]
5. Li, J.; Zhang, S.; Feng, Q.; Wang, X.; Wu, Z.; Sun, B. Simulation Analysis and Field Verification of Static Evaporation Characteristics of Full-Scale LNG Storage Tanks. *Appl. Therm. Eng.* **2024**, *253*, 123721. [[CrossRef](#)]
6. Luan, X.; Zhang, M.; Zhao, S.; Zhang, B. Numerical Study on the Effects of Bund on Liquid Pool Spreading and Vapor Dispersion after a Catastrophic LNG Tank Failure. *Process Saf. Environ. Prot.* **2023**, *176*, 74–86. [[CrossRef](#)]
7. Mocellin, P.; Pio, G.; Carboni, M.; Pilo, F.; Vianello, C.; Salzano, E. On the Effectiveness of Mitigation Strategies for Cryogenic Applications. *J. Loss Prev. Process Ind.* **2023**, *84*, 105123. [[CrossRef](#)]
8. Carboni, M.; Pio, G.; Mocellin, P.; Vianello, C.; Maschio, G.; Salzano, E. Accidental Release in the Bunkering of LNG: Phenomenological Aspects and Safety Zone. *Ocean. Eng.* **2022**, *252*, 111163. [[CrossRef](#)]
9. Sun, D.; Wang, C.; Shen, Q. A Compression-Free Re-Liquefaction Process of LNG Boil-off Gas Using LNG Cold Energy. *Energy* **2024**, *294*, 130894. [[CrossRef](#)]
10. GIIGNL Technical Study Group LNG. *Custody Transfer Handbook*; Information Paper No. 1; GIIGNL: Neuilly-sur-Seine, France, 2015; Volume 5.
11. Lee, J.N.; Kawabata, K.; Bang, C.S.; Joh, K.H.; Ha, M.K. A Method for the Prediction of Heat Capacity of LNG Cargo Tanks during Cool-down and Warm-Up. In Proceedings of the SNAME Maritime Convention, Houston, TX, USA, 15–17 October 2008.
12. Chen, Q.; Wegrzyn, J. Analysis of Temperature and Pressure Changes in Liquefied Natural Gas (LNG) Cryogenic Tanks. *Cryogenics* **2004**, *44*, 701–709. [[CrossRef](#)]
13. Keefer, K.A.; Hartwig, J. Development and Validation of an Analytical Charge-Hold-Vent Model for Cryogenic Tank Chillover. *Int. J. Heat. Mass. Transf.* **2016**, *101*, 175–189. [[CrossRef](#)]
14. Zhang, S.; Huang, Z.; Li, G.; Wu, X.; Peng, C.; Zhang, W. Numerical Analysis of Transient Conjugate Heat Transfer and Thermal Stress Distribution in Geothermal Drilling with High-Pressure Liquid Nitrogen Jet. *Appl. Therm. Eng.* **2018**, *129*, 1348–1357. [[CrossRef](#)]
15. Dong, H.; Xu, Q. Finite Element Analysis on the Thermal Stress of LNG Carriers' Tanks. *Chem. Eng. Trans.* **2018**, *67*, 793–798.
16. Hwang, S.Y.; Kim, M.S.; Lee, J.H. Thermal Stress Analysis of Process Piping System Installed on LNG Vessel Subject to Hull Design Loads. *J. Mar. Sci. Eng.* **2020**, *8*, 926. [[CrossRef](#)]
17. Wang, B.; Zhang, Z.; Huang, K.; Zhang, Y.; Zhang, Z.; Gao, H.; Fu, L. Stress and Pressure Pulsation Analysis of Low Temperature Compressor Piping System in LNG Vaporizing Station. *Energies* **2022**, *15*, 1874. [[CrossRef](#)]
18. Lee, J.H.; Kim, Y.J.; Hwang, S. Computational Study of LNG Evaporation and Heat Diffusion through a LNG Cargo Tank Membrane. *Ocean. Eng.* **2015**, *106*, 77–86. [[CrossRef](#)]
19. Wang, C.; Ju, Y.; Fu, Y. Dynamic Modeling and Analysis of LNG Fuel Tank Pressurization under Marine Conditions. *Energy* **2021**, *232*, 121029. [[CrossRef](#)]
20. Kang, Z.; Yanzhong, L.; Yuan, M.; Lei, W.; Fushou, X.; Jiaojiao, W. Experimental Study on Cool down Characteristics and Thermal Stress of Cryogenic Tank during LN<sub>2</sub> Filling Process. *Appl. Therm. Eng.* **2018**, *130*, 951–961. [[CrossRef](#)]
21. Zhu, K.; Li, Y.; Ma, Y.; Wang, J.; Wang, L.; Xie, F. Influence of Filling Methods on the Cool down Performance and Induced Thermal Stress Distribution in Cryogenic Tank. *Appl. Therm. Eng.* **2018**, *141*, 1009–1019. [[CrossRef](#)]
22. Lu, J.; Xu, S.; Deng, J.; Wu, W.; Wu, H.; Yang, Z. Numerical Prediction of Temperature Field for Cargo Containment System (CCS) of LNG Carriers during Pre-Cooling Operations. *J. Nat. Gas. Sci. Eng.* **2016**, *29*, A1–A16. [[CrossRef](#)]
23. Zhang, C.; Chen, F.; Wang, Y.; Peng, Y.; Zhao, Y.; Lv, M. A Study on Temperature-Stress Model of Pre-Cooling for Re-Condenser in LNG Receiving Station. *AIP Adv.* **2020**, *10*, 065322. [[CrossRef](#)]
24. Shin, K.; Son, S.; Moon, J.; Jo, Y.; Kwon, J.S.-I.; Hwang, S. Dynamic Modeling and Predictive Control of Boil-off Gas Generation during LNG Loading. *Comput. Chem. Eng.* **2022**, *160*, 107698. [[CrossRef](#)]
25. Lim, Y.K.; Lee, S.G.; Ko, M.; Park, K.; Lee, J.M. Operational Strategy of Pre-Cooling Process of CO<sub>2</sub> Storage Tank in CCS Ship Transportation Using Model-Based Optimization. *Chem. Eng. Res. Des.* **2016**, *109*, 770–779. [[CrossRef](#)]
26. Kulitsa, M.; Wood, D. Boil-off Gas Balanced Method of Cool down for Liquefied Natural Gas Tanks at Sea. *Adv. Geo-Energy Res.* **2020**, *4*, 199–206. [[CrossRef](#)]
27. Ansys. *Ansys Fluent Theory Guide*; ANSYS, Inc.: Canonsburg, PA, USA, 2020; R1.
28. Payri, R.; Gimeno, J.; Martí-Aldaraví, P.; Alarcón, M. A New Approach to Compute Temperature in a Liquid-Gas Mixture. Application to Study the Effect of Wall Nozzle Temperature on a Diesel Injector. *Int. J. Heat. Fluid. Flow.* **2017**, *68*, 79–86. [[CrossRef](#)]
29. Charton, H.; Perret, C.; Phan, H.T. Analysis of Supersonic Flows inside a Steam Ejector with Liquid–Vapor Phase Change Using CFD Simulations. *Thermo* **2024**, *4*, 1–15. [[CrossRef](#)]
30. Wu, J.; Cai, J.; Yuan, S.; Zhang, X.; Reniers, G. CFD and EnKF Coupling Estimation of LNG Leakage and Dispersion. *Saf. Sci.* **2021**, *139*, 105263. [[CrossRef](#)]
31. Saleem, A.; Farooq, S.; Karimi, I.A.; Banerjee, R. A CFD Simulation Study of Boiling Mechanism and BOG Generation in a Full-Scale LNG Storage Tank. *Comput. Chem. Eng.* **2018**, *115*, 112–120. [[CrossRef](#)]
32. NIST Nitrogen-NIST Chemistry WebBook. Available online: <https://webbook.nist.gov/cgi/cbook.cgi?ID=C7727379&Units=SI&Mask=4#Thermo-Phase> (accessed on 15 February 2024).

33. NIST Methane-NIST Chemistry WebBook. Available online: <https://webbook.nist.gov/cgi/cbook.cgi?ID=C74828&Units=SI&Mask=4#Thermo-Phase> (accessed on 15 February 2024).
34. Koopman, R.P. Analysis of Burro Series 40-M3 Lng Spill Experiments. *J. Hazard. Mater.* **1982**, *6*, 43–83. [[CrossRef](#)]
35. Bellegoni, M.; Chicchiero, C.; Landucci, G.; Galletti, C.; Salvetti, M.V. A UQ Based Calibration for the CFD Modeling of the Gas Dispersion from an LNG Pool. *Process Saf. Environ. Prot.* **2022**, *162*, 1043–1056. [[CrossRef](#)]
36. Kim, S.Y.; Ahn, Y.; Kim, K.H.; Kim, Y.; Korea, S.; Heo, J.H.; Jeong, T.; Lee, C.H.; Kim, D.H. Experimental Studies on Sloshing in a Stx Independence Type-B Tank. In Proceedings of the International Offshore and Polar Engineering Conference, Anchorage, AK, USA, 30 June–5 July 2013.
37. Dong, W.; Zhang, Z.; Liu, J.; Xie, D. Strength Assessment on Support System of LNG Independent Type B Tank under Sloshing Loads. In Proceedings of the International Conference on Offshore Mechanics and Arctic Engineering—OMAE, Trondheim, Norway, 25 June–1 July 2017; Volume 3B.

**Disclaimer/Publisher’s Note:** The statements, opinions and data contained in all publications are solely those of the individual author(s) and contributor(s) and not of MDPI and/or the editor(s). MDPI and/or the editor(s) disclaim responsibility for any injury to people or property resulting from any ideas, methods, instructions or products referred to in the content.